UNIVERSITAT DE BARCELONA

Contractile response of alveolar epithelial cells to biochemical or mechanical stimulation probed by traction microscopy

Núria Gavara i Casas

Contractile response of alveolar epithelial cells to biochemical or mechanical stimulation probed by traction microscopy

A dissertation by
Núria Gavara i Casas
in partial fulfilment of the requirements for
the degree of Doctor of Philosophy

Thesis supervisor : Prof. Ramon Farré i Ventura

Unitat de Biofísica i Bioenginyeria
Dept. de Ciències Fisiològiques I
Facultat de Medicina, Universitat de Barcelona.

Chapter 4. Thrombin-induced contraction in alveolar epithelial cells probed by traction microscopy.

4.1 Introduction

The alveolar epithelium forms a semipermeable barrier between the alveolar airspace and the lung interstitium. The epithelial cell monolayer enables gas exchange but restricts movement of liquid, macromolecules and cells into the alveoli. A key feature of acute lung injury (ALI) is alveolar flooding and infiltration of leukocytes into the alveolar compartment (Matthay and Zimmerman, 2005;Ware and Matthay, 2000). Enhanced permeability of the alveolar barrier in ALI has been associated with disruption of the cell monolayer by formation of gaps between adjacent cells (Ware and Matthay, 2000;Matthay and Zimmerman, 2005). Therefore, preservation of the physical integrity of the cell monolayer is a critical requirement for maintenance of epithelial barrier function.

Alveolar epithelial cells are mechanically attached to each other and to the extracellular matrix by means of anchoring junctions. The physical integrity of the cell monolayer is governed by a dynamic force balance at the cell-cell and cell-matrix attachments between centripetal cell mechanical tension and centrifugal adhesive forces (Moy et al., 1996;Dudek and Garcia, 2001). Mechanical tension arises from both active contraction generated by the acto-myosin machinery and passive elastic recoil caused by cyclic stretching due to breathing or mechanical ventilation. Maintenance of the cell monolayer requires tethering adhesive forces to withstand active and passive tension.

Chapter 4 Thrombin-induced contraction in alveolar epithelial cells probed by traction microscopy.

Thrombin is a serine protease which plays a key role in the coagulation cascade (Macfarlane et al., 2001). In addition, thrombin has been associated with endothelial barrier dysfunction (An et al., 2005;Bogatcheva et al., 2002;Dudek and Garcia, 2001). Cultured endothelial cell monolayers show increased permeability after thrombin addition, which is indicative of monolayer disruption with leakage of liquid and macromolecules through paracellular gaps (Amerongen et al., 2000). The detachment between adjacent cells has been attributed to a rise in contractile activation and loss of cell-cell adhesion (Bogatcheva et al., 2002;Dudek and Garcia, 2001;Moy et al., 2002). Endothelial barrier disruption may allow the passage of thrombin into the interstitial space, stimulating alveolar epithelial cells at the sites of lung inflammation. Nevertheless, the effect of thrombin in epithelial barrier function remains unclear. Kawkitinarong and coworkers (Kawkitinarong et al., 2004) recently found increased transepithelial electrical resistance (TER) of alveolar epithelial cell monolayers in response to thrombin. These authors suggested a barrier protective effect of thrombin in alveolar epithelial cells, which contrasts with the disruptive response found in endothelial cells. Enhancement of epithelial barrier function reflects changes in the cell force balance. We have recently observed that thrombin stiffens alveolar epithelial cells (Trepat et al., 2005), which could result in increased internal elastic tension. In addition, thrombin has been shown to enhance myosin light chain (MLC) phosphorylation in alveolar epithelial cells (Kawkitinarong et al., 2004), which could lead to a further increase in the centripetal tension applied to the cell attachments. The barrier protective effect of thrombin reported in alveolar epithelial cells could be explained by a strengthening of cell adhesion that counterbalances an increase in centripetal forces (Kawkitinarong et al., 2004). However, thrombin induces a cortical ring with formation of actin bundles in alveolar epithelial cells (Trepat et al., 2005;Kawkitinarong et al., 2004). This cytoskeleton remodeling could result in a more tangential direction of contractile peripheral tension, thereby reducing the net disruptive force imposed on the cell adhesions. Therefore, direct measurements of the magnitude and direction of the contractile forces applied by the cell to the external attachments are necessary to better define the effect of thrombin in the force balance that regulates alveolar barrier permeability in lung inflammation. Traction microscopy (TM) is a recently developed technique to probe cell contraction (Butler et al., 2002;Dembo and Wang, 1999). TM allows us to measure the regional distribution of contraction forces and the time course of the contractile response to pharmacological stimuli at the single cell level.

The aim of this work was to study thrombin-induced contractile forces of alveolar

epithelial cells by traction microscopy. Single alveolar epithelial cells (A549) were challenged with thrombin and the time course of traction forces exerted on the substrate was measured by TM. Contribution of actin polymerization to thrombin-induced contraction was assessed by pretreating the cells with cytochalasin D. The role of MLC kinase (MLCK) and Rho kinase pathways of MLC phosphorylation in cell contraction was evaluated by inhibiting these signaling pathways with ML-7 and Y-27632, respectively. F-actin and G-actin staining were used to assess structural changes in actin cytoskeleton.

4.2   Materials and methods

4.2.1   Materials

Tissue culture medium RPMI 1640, L-glutamine, penicillin and streptomycin were obtained from GIBCO (Gaithersburg, MD), fetal calf serum from Biological Industries (Kibbutz Beit Haemek, Israel) and collagen I from Upstate (Lake Placid, NY). Unless otherwise specified, reagents were purchased from Sigma Chemical Co. (St. Louis, MO). Acrylamide, bis-acrylamide and ammonium persulfate were obtained from Bio-Rad laboratories (Hercules, CA). Fluorescent latex beads and Alexa Fluor 488 DNase I conjugate were supplied by Molecular Probes (Eugene, OR). Repel silane was obtained from Amersham Biosciences.

4.2.2   Cell culture

The study was carried out on human alveolar epithelial cells A549 (culture line CCL-185 ATCC, Manassas, VA). Cells were cultured in HEPES buffered RPMI 1640 medium supplemented with 10% inactivated fetal calf serum, 1mM L-glutamine, 100 U/ml penicillin, 100 mg/ml streptomycin and 2 µg/ml amphotericin B. Two days before traction microscopy experiments cells were detached by means of a brief exposure to trypsin EDTA and plated sparsely on polyacrylamide gel disks (2500 cells/disk), which had previously been coated with 400 µg/ml rat tail collagen I. The culture medium was replaced by serum-free medium 24 h after plating. For actin staining, cells were plated on 12 mm diameter cover slips 24 hours before experiments (15000 cells/cover slip).

4.2.3 Polyacrilamide gels

Preparation of polyacrylamide gels.

Preparation of thin collagen-coated polyacrylamide gel disks was carried out as described by Pelham and Wang (Pelham, Jr. and Wang, 1999). Green fluorescent latex beads 0.2 $\llcorner$ m in diameter were mixed with 2% acrylamide and 0.3% bis-acrylamide solution (1:125 vol/vol bead solution volume of acrylamide mixture). Gel disks ~70 μm thick and 8 mm in diameter attached to a glass coverslip were prepared with 5.5 μl of this solution and subsequently coated with 3 μg/cm^2 collagen I. The extended protocol for preparation of collagen I coated polyacrilamide gels is described in Appendix X.

Measurement of Young's modulus of the polyacrylamide gels

Young's modulus (*E*) of polyacrylamide gels was measured with atomic force microscopy using a triangular cantilever with a pyramidal tip (Mikromasch, Tallin, Estonia) as previously described (Alcaraz et al., 2003;Rico F, 2005). The spring constant of the atomic force microscopy cantilever was calibrated by the thermal fluctuations method in water (Burnham et al., 2003). Force-displacement curves (1-μm indentation at 1Hz) were recorded at four distant points on the surface of four gel samples. E was computed from the force-displacement curves (Bilodeau, 1992) using nonlinear least squares regression. For each gel sample, the value of E was taken as the average of the four measurements done at different surface points. The coefficient of variation (SD/mean) of E within samples was on average 23%. E of the gel samples was E = 65 ± 114 Pa (mean ± SD). Variability between samples (coefficient of variation = 31%) was comparable with intrasample variability. The average E measured in the gels was used for computing cell traction forces from bead displacement measurements.

Microscopy.

Cover slips containing cell-cultured polyacrylamide disks were mounted on the stage of an inverted fluorescence microscope (Eclipse TE2000, Nikon, Japan) placed on a vibration isolation table (Isostation, Newport, Irvine, CA). Bright field and fluorescence images were acquired with a 12-bit resolution cooled-CCD camera (Orca AG, Hamamatsu Photonics, Japan). The apparent pixel size after magnification (40×) was 0.16 μm with a resulting field of view of 161×161 μm^2.

4.2.4 Actin staining

The protocol for F- and G-actin staining is extensively described in Appendix X. F/G-actin fluorescence ratio was quantified using fields containing >30 cells imaged with an inverted fluorescence microscope (Eclipse TE2000, Nikon) and a 12-bit-resolution cooled-charge-coupled device camera (Orca, Hamamatsu Photonics) at 10× magnification. As a positive control of this technique in A549 cells, we obtained a 14-fold decrease in F/G-actin fluorescence ratio after Latrunculin A treatment (2 µm). F-actin cytoskeleton imaging was performed with a confocal laser scanning microscope (TCS-NT; Leica Microsystems, Heidelberg, Germany) at 63× magnification.

4.2.5 Measurements

A gel disk with cultured A549 cells was placed in the microscope and imaged with bright field illumination. A bright field image of an isolated cell was captured to determine its boundary. Subsequently, the apical surface of the gel was focused and fluorescence images of the microbeads embedded near the surface of the gel were acquired at 1 image/min. After 5 minutes of baseline recording, thrombin (final concentration 1 U/ml) or vehicle (control) was added and fluorescent images were acquired for 10 additional minutes. At the end of the recording, a bright field image was captured and the cells were removed from the gel by exposure to trypsin. Finally, an additional fluorescent image was recorded to determine the position of the beads in the unstrained gel (reference image). Measurements were taken in n = 12 cells from different cell-gel samples for thrombin and vehicle experiments. 12 % of isolated cells showed partial detachment from the substrate after thrombin addition. Thrombin detached cells were discarded for TM measurements. The role of the actin cytoskeleton in the thrombin-induced contraction was studied by pretreating the cell culture with cytochalasin D (5 µM) for 30 minutes prior to thrombin treatment. The time-course of the response to thrombin was measured (n = 12) as described above. The role of MLCK and Rho-kinase signalling pathways of MLC phosphorylation was studied by pretreating the cell culture with ML-7 (10 µM, n = 12) or Y-27632 (10 µM, n = 12) 30 minutes prior thrombin challenge.

Polymerization and rearrangement of the actin cytoskeleton was assessed by staining of F- and G-actin of cells cultured on glass cover slips. Staining protocol is

extensively described in Appendix X. Staining was carried out 10 min after adding thrombin (1 U/ml) or vehicle. Images were taken in n = 15 cover slips for each treatment. The actin cytoskeleton was also studied in cells treated (10 min) with thrombin (1 U/ml) or vehicle after pretreatment for 30 min with cytochalasin D (5 µM, n = 15), ML-7 (10 µM, n = 15) or Y-27632 (10 µM, n = 15).

4.2.6 Traction microscopy data processing

Cell boundary was determined using a Sobel edge detector algorithm (Castleman KR, 1996) implemented in LabView (National Instruments, Austin, TX). The projected area of the cell (A) was computed as the area enclosed by the cell boundary. The centroid was computed as the center of mass of the projected area of the cell. Cell speed was computed as the displacement of the centroid between the initial and final bright field images divided by the elapsed time. To compute traction forces (T) exerted by the cell on the substrate, the displacement field of the gel substrate was first determined from the stored fluorescent bead images. The displacement field between each fluorescence image and the reference image was computed using the Image Correlation Method (Tolic-Norrelykke et al., 2002). Images were iteratively divided into smaller windows and the displacement field between a pair of images was obtained by identifying the coordinates of the peak of the cross-correlation function between each pair of windows. The traction field ($T(x,y)$) was computed from the gel Young's modulus and the displacement field using Constrained Fourier Transform Traction Cytometry (CFTTC) (Butler et al., 2002). In traction field computations, the cell boundary estimated with the edge detector algorithm was enlarged by 3 µm, to ensure that the computed contour encompassed the entire cell edge. Cells with unclear boundary or displacement fields incongruent with cell shape were rejected. The spatial resolution of the displacement and traction maps was 1.3 µm.

For each traction field, the total force magnitude (F) was computed by integrating the magnitude of $T(x,y)$ over the projected area of the cell (Gaudet et al., 2003). Although the net vectorial force over the contact area is zero, the integral of the modulus provides a useful index of the cell contractile strength. The average traction of the cell was computed as F/A. Orientation of the traction force at each point was assessed as the angle between the traction vector and the vector pointing towards the centroid of the projected area of

the cell (Fig. 4.3 inset). The spatial distribution of traction forces was assessed by dividing the projected area of the cell into 5 adjacent regions (1.26 µm thick) containing points progressively distant from the cell edge. We computed the average traction magnitude in each of these 5 adjacent bands (distant 0, 1.26, 2.52, 3.78, 5.04 µm from the cell edge) and in the remaining central region (distant 6.3 µm) (Fig. 4.4 inset). The net contractile moment (M) was computed as defined by Butler and coworkers (Butler et al., 2002). M is a measure of the cell contractile strength that can be used as an index of cytoskeleton tensile stress (prestress) (Wang et al., 2002). The polarity of cell contraction was defined as M_{xx}/M, where M_{xx} is the contractile moment along the principal axis of contraction (Butler et al., 2002).

4.2.7 Statistics

Unless stated otherwise, data are reported as mean ± SE. For time-course experiments, baseline data were taken as the average of the last 3 values measured before adding thrombin or vehicle. Posttreatment data were taken as the average of the values measured between 8 and 10 min after treatment. Comparisons between two groups were carried out by paired or unpaired Student t-test for dependent or independent samples, respectively. Statistical significance was assumed at $P < 0.05$.

4.3 Results

4.3.1 Mapping of cell contraction.

Displacement and traction fields of an A549 cell before and after thrombin addition are shown in Fig. 4.1. Under baseline conditions the cell exhibited a modest contractile tone with weak traction forces mainly located along the cell periphery, heterogeneously distributed and pointed towards the nucleus. Little traction was observed beneath the central region of the cell. Thrombin induced a marked increase in cell contraction. Force distribution and direction remained similar to baseline tone with the highest force increase at cell edges.
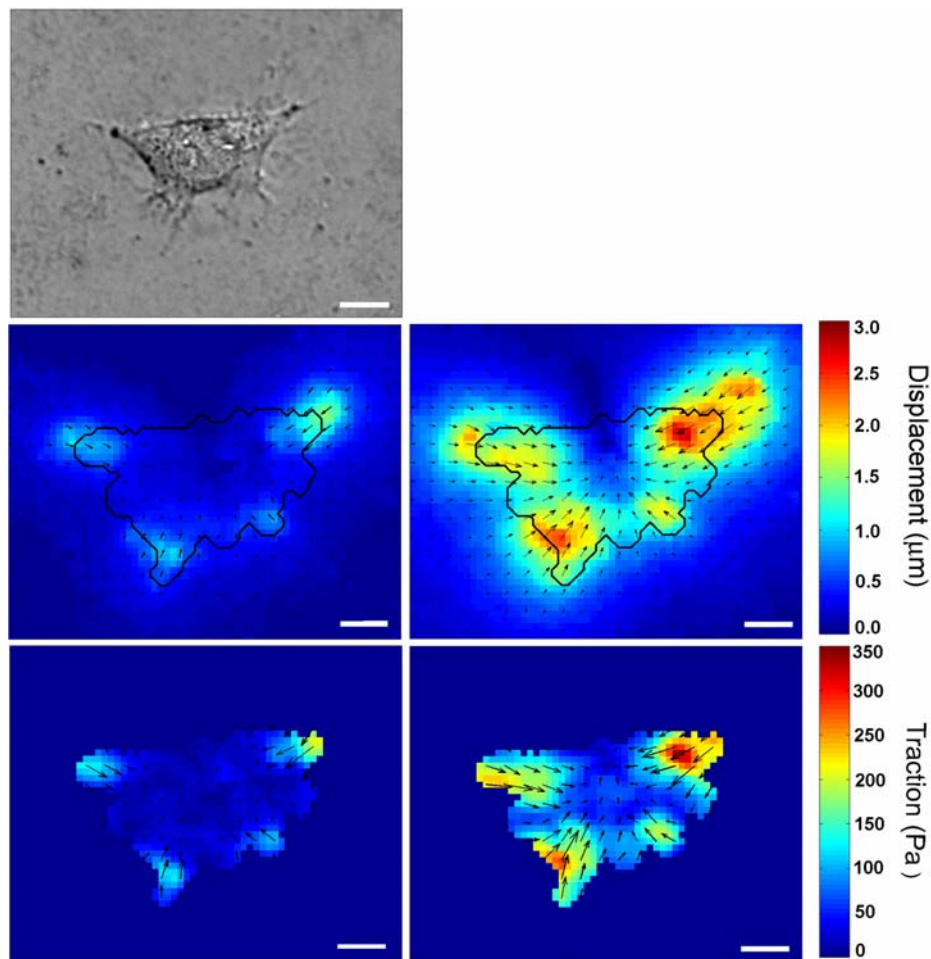
Fig. 4.1 Mapping of alveolar epithelial cell contraction induced by thrombin. Bright field image of an A549 cell before thrombin stimulation (top). Displacement field (mid) and corresponding traction field (bottom) of the cell before (left) and 10 min after thrombin addition (1 U/ml) (right). Cell boundary drawn from the bright field image is shown as a black line. Color scales indicate the magnitude of displacement (mid) and traction force

4.3.2 Effect of thrombin on cell contraction and the actin cytoskeleton.

Total force magnitude of A549 cells under baseline conditions was 55.0 ± 12.0 nN with maximal local traction of 157.0 ± 17.3 Pa. (Fig. 4.2) The area of cells was 993 ± 57 μm^2 corresponding to an average traction of 37.0 ± 5.0 Pa. Cell speed of control cells was 42.4 ± 8.3 nm/min. Thrombin caused a fast and sustained 2.5-fold increase in
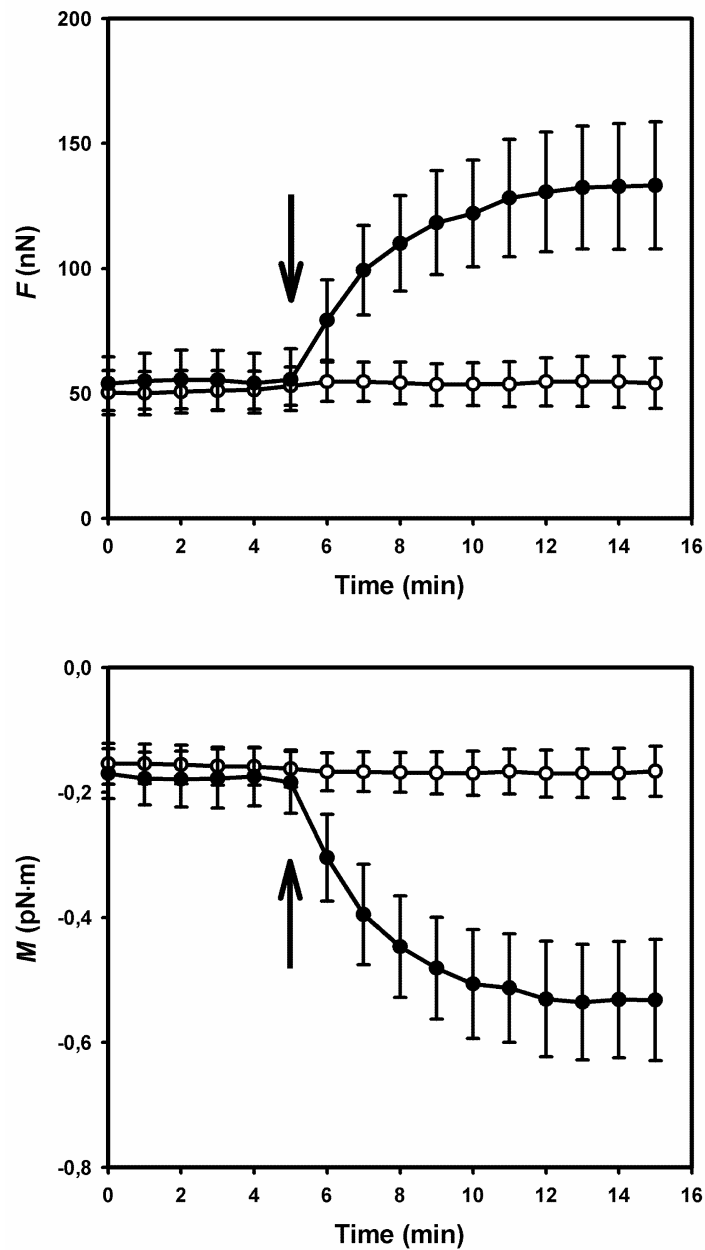
Fig. 4.2 Time course of contractile response of alveolar epithelial cells challenged with thrombin (closed symbols) or vehicle (open symbols). Top: Total force magnitude (F). Bottom: Net contractile moment (M). The arrows indicate addition of thrombin (final concentration 1 U/ml; n = 12) or vehicle (n = 12). Data are mean ± SE. Adapted from (Gavara et al., 2006).

rise was found in average traction (F/A) (P < 0.001). Thrombin addition resulted in a maximal local traction of 280.2 ± 26.6 Pa (P < 0.001). No significant change in F and M was observed when vehicle was added to cells (Fig. 4.2). Baseline traction at the cell periphery was 45.2 ± 5.7 Pa and decreased by 50 % in the central region of the cell (Fig. 4.4). After thrombin addition, a similar rise in traction (~2.5-fold) was observed in the periphery and the center of the cell. The distribution of traction orientation was very well fitted with a Gaussian fit with a small additional constant term accounting for the traction field noise (Fig. 4.3). Under baseline conditions, the Gaussian distribution was relatively narrow (SD = 37.3 degree) and centered around zero (mean = -1.3 degree), indicating a predominant centripetal orientation of the contractile tone of the cells. Thrombin resulted in a sharper Gaussian distribution (SD = 23.3 degree) centered around zero (mean = -1.7 degree), indicating enhanced centripetal orientation of cell contraction. Under baseline conditions the contractile moment along the principal axis of contraction was ~3/4 of the net contractile moment (M_{xx}/M = 0.78 ± 0.03). Thrombin did not cause significant changes in cell contraction polarity.

F-actin staining of vehicle-treated cells showed a diffuse pattern (Fig. 4.5). Thrombin caused rearrangement of the F-actin cytoskeleton with formation of a marked peripheral rim (Fig. 4.5). F-actin staining of single cells showed actin organization similar to that of confluent cells (Fig. 4.5, insets). F/G actin fluorescence ratio was 4.0 ± 0.4 in vehicle-treated cells. The ratio increased by 27% (P < 0.05) in thrombin-challenged cells Fig. 4.6.

4.3.3   Role of the actin cytoskeleton in cell contraction.

Disruption of the actin cytoskeleton with cytochalasin D decreased the baseline contractile force by 47% (P < 0.01) (Fig. 4.7). Traction force induced by thrombin in cytochalasin D pretreated cells was 3.5-fold lower than in non-pretreated cells (P < 0.01). No significant changes in F/G actin fluorescence ratio were found in cells pretreated with cytochalasin D and subsequently treated with vehicle or thrombin (Fig. 4.6). Disruption of the actin cytoskeleton was evident in F-actin distribution (Fig. 4.8). Disappearance of actin structures was associated with irregularly polymerized actin aggregates throughout the cytoplasm. Thrombin addition did not modify this pattern.
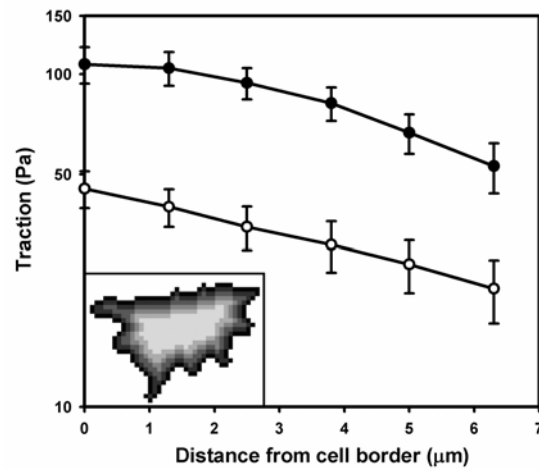
Fig. 4.4 Spatial distribution of traction forces. Average traction within adjacent bands (1.26 µm thick) parallel to the cell boundary and within the central region containing points whose distance is > 6.3 µm from the cell boundary at baseline (open symbols) and after thrombin addition (closed symbols). Data are mean ± SE. Inset: Adjacent bands computed in a representative cell. Adapted from (Gavara et al., 2006).
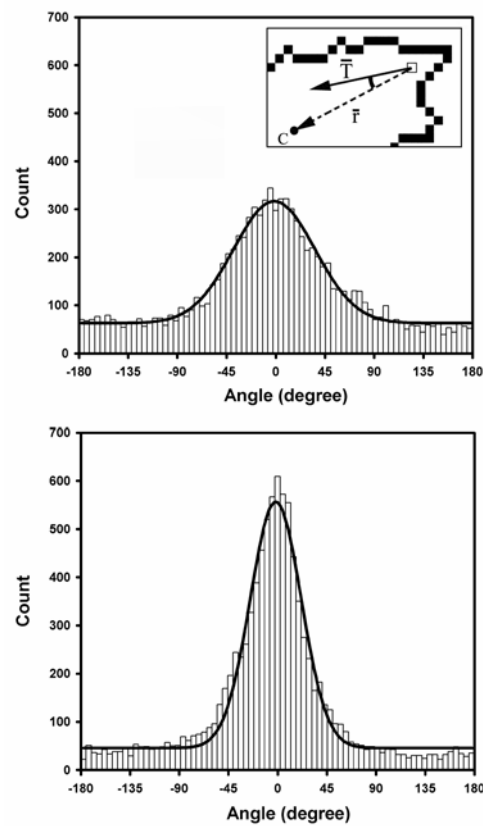
Fig. 4.3 Histograms of centripetal orientation of contractile forces at baseline (top) and after thrombin addition (bottom). Plots are pooled traction data of n = 12 cells. Thick solid lines are fit of a Gaussian distribution with an additional constant term. Inset: sketch of angle definition. T and r represent the traction vector and the vector pointing towards the centroid (C) of the cell, respectively. Adapted from (Gavara et al., 2006).

65

Fig. 4.5. Actin cytoskeleton remodeling induced by thrombin on alveolar epithelial cells. F-actin staining with phalloidin-TRITC 10 min after adding vehicle (top) or thrombin (1 U/ml) (bottom). Insets show F-actin staining of single cells.

4.3.4 Role of inhibition of MLCK and Rho kinase in cell contraction.

Inhibition of MLCK with ML-7 decreased baseline traction force of alveolar epithelial cells by 76 % (P < 0.01) (Fig. 4.7). A simil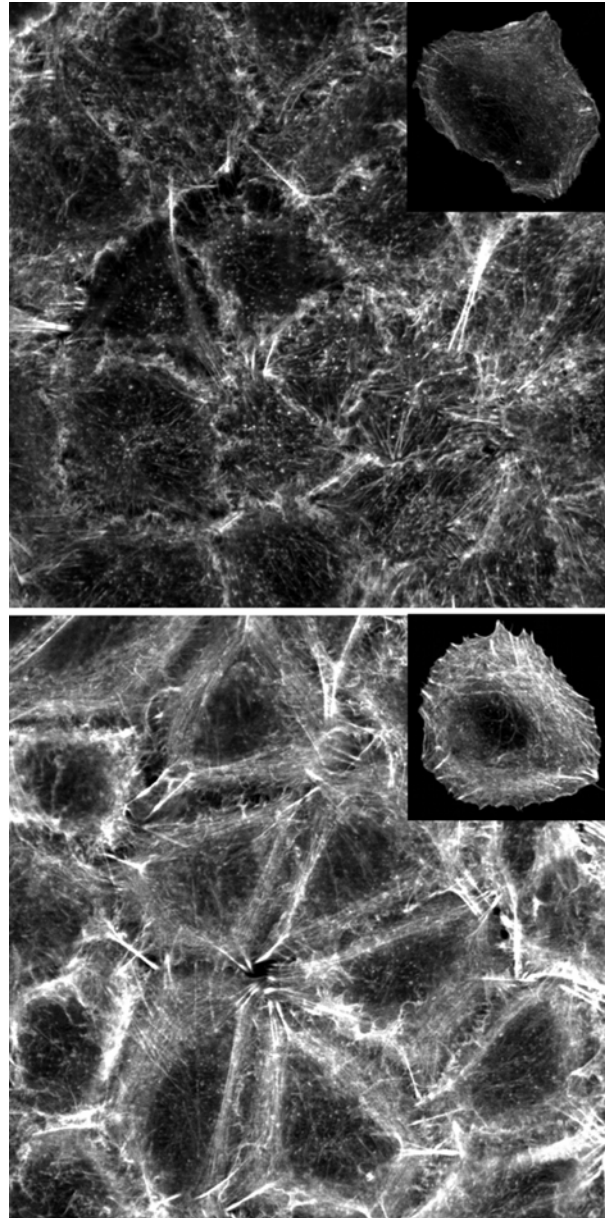ar relaxation of baseline force (74 %, P < 0.01) was obtained when Rho kinase was inhibited with Y-27632. Traction force after thrombin challenge was 6-fold lower (P < 0.001) when cells were pretreated with either ML-7 or Y-27632.

No changes in F/G actin fluorescence ratio were observed when MLCK was inhibited with ML-7 (Fig. 4.6). Thrombin caused a G-actin to F-actin conversion (21%, P < 0.05) similar to that observed in cells without MLCK inhibition. Pretreatment with ML-7 did not modify F-actin distribution (Fig. 4.8). Similarly, inhibition of MLCK did not reduce the thrombin-induced formation of a peripheral rim of actin bundles.

Fig. 4.6 Effect of disruption of the actin cytoskeleton and inhibition of MLCK and Rho-kinase on the conversion of G-actin to F-actin induced by thrombin in alveolar epithelial cells. F/G actin fluorescent ratio of cells challenged with vehicle (open bars) or thrombin (filled bars) non-pretreated or pretreated (30 min) with cytochalasin D (5 µM), ML-7 (10 µM) and Y-27632 (10 µM). Data are plotted as mean ± SE (n = 15). + and ++ indicate P < 0.05 and P < 0.01, respectively, compared with non-pretreated cells challenged with thrombin. Differences between pretreated and non pretreated cells challenged with vehicle were not significant. Adapted from (Gavara et al., 2006).

Inhibition of Rho-kinase did not significantly change F/G actin fluorescence ratio (Fig. 4.6). Thrombin-induced polymerization of F-actin was lower on cells pretreated with Y-27632 (12%) but did not attain significance (P = 0.29). Inhibition of Rho-kinase slightly modified F-actin cytoskeleton, resulting in a more diffuse actin distribution (Fig. 4.8). Thrombin did not induce actin bundle formation in cells pretreated with Y-27632
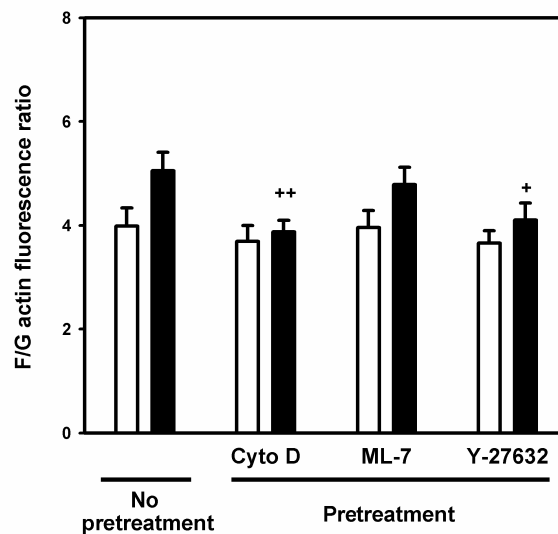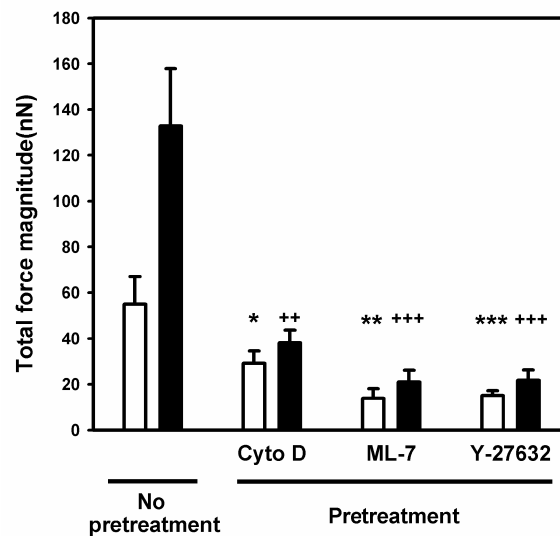

Fig. 4.7 Effect of disruption of the actin cytoskeleton and inhibition of MLCK and Rho-kinase on the contractile response induced by thrombin in alveolar epithelial cells. Baseline (open bars) and thrombin-induced (filled bars) total force magnitude of cells non-pretreated and pretreated (30 min) with cytochalasin D (5 µM), ML-7 (10 µM) and Y-27632 (10 µM). Data are plotted as mean ± SE (n = 12). *, ** and *** indicate P < 0.05, P < 0.01 and P < 0.001, respectively, compared with baseline of non-pretreated cells. ++ and +++ indicate P < 0.01 and P < 0.001, respectively, compared with thrombin-induced force of non-pretreated cells. Adapted from (Gavara et al., 2006).
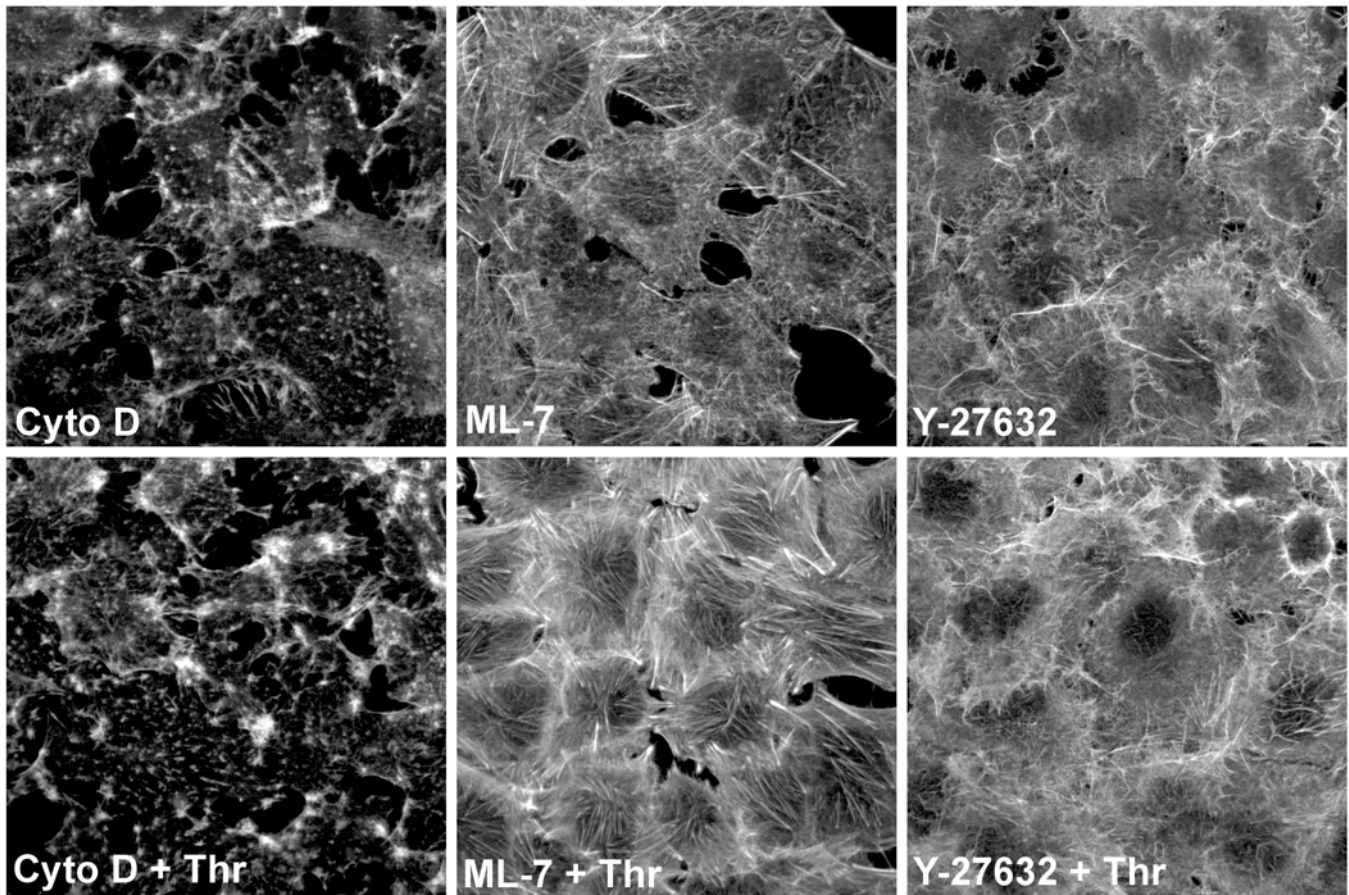
Fig. 4.8 Effect of disruption of the actin cytoskeleton and inhibition of MLCK and Rho-kinase on the actin remodeling induced by thrombin in alveolar epithelial cells. F-actin staining with phalloidin-TRITC 10 min after adding vehicle (top) or thrombin (1U/ml) (bottom). Cells were pretreated with cytochalasin D (5 µM) (left), ML-7 (10 µM) (mid) and Y-27632 (10 µM) (right) for 30 minutes prior to thrombin challenge. Adapted from (Gavara et al., 2006).

4.4 Discussion

This study demonstrates that thrombin induces fast and marked contraction of A549 alveolar epithelial cells. The distribution of traction forces before and after thrombin challenge was mainly located along the cell periphery and pointed towards the cell center. Thrombin caused actin polymerization and enhancement of the peripheral actin rim. Disruption of the actin cytoskeleton and reduction of MLC phosphorylation by inhibition of MLCK or Rho-kinase activities attenuated both the basal contractile state of the cell and the thrombin-induced contractile response.

4.4.1 Methods to probe cell contractile forces

Cell contraction can be readily probed by plating cells on top of a soft elastic gel or casting them inside the gel (Fang et al., 2004;Kolodney and Wysolmerski, 1992;Moy et al., 2002;Umino et al., 2000). Contractile cell response to pharmacological stimulation can be assessed with force transducers attached to the gel (Kolodney and Wysolmerski, 1992;Moy et al., 1996) or by measuring the reduction in the gel area (Fang et al., 2004;Umino et al., 2000). These approaches enable assessment of relative changes in average contraction strength of the cell culture. However, measurement of force or deformation of the bulk gel does not allow accurate determination of the baseline contractile tone or the regional distribution and absolute magnitude of contractile forces at the single cell level. By contrast, traction microscopy maps local gel deformations by tracking the displacement of small fluorescent beads embedded in the gel. By removing the cells attached to the surface of the gel at the end of the experiment, the relaxed position of the beads in unstrained gel is easily determined. Moreover, in contrast with microfabricated pillar-array techniques (Tan et al., 2003), the stiffness of the substrate and the spatial force resolution can be easily tuned to each particular cell type. Thus, traction microscopy enabled measurement of the time course of the absolute magnitude and regional distribution of forces exerted by single alveolar epithelial cells with micrometric spatial resolution. TM requires cell contractile forces to be balanced solely by the gel through cell-substrate attachments. Therefore, TM measurements were made on isolated adherent cells that lack cell-cell attachments. In

confluent cell monolayers contractile forces are in part offset by cell-cell tethering forces, thus reducing the contribution of cell-matrix adhesions.

4.4.2   A549 as a model of alveolar epithelial cells

The A549 is a cell line derived from human bronchoalveolar cell carcinoma. These cells are widely used as a model of alveolar epithelial cells in vitro because they are readily cultured and retain important features of type II alveolar cells (Lieber M, 1976). In particular, it has been recently shown that this cell type forms a tight monolayer when grown to confluence and that the barrier permeability is modulated by thrombin (Kawkitinarong et al., 2004). Moreover, A549 cells displayed ability similar to that of primary rat type II cells to contract collagen gels (Umino et al., 2000). Cell speed of the isolated A549 cells was 25-fold smaller than that reported for migrating cell types (Dallon and Othmer, 2004). Moreover, immunofluorescence images of isolated A549 cells did not display front-rear polarity of the F-actin cytoskeleton (Fig 5, inset). These results indicate that the A549 cells studied in TM experiments adopted a non-migrating behavior. The low motility exhibited by the A549 cells could be attributed to the high concentration of type I collagen used to coat the polyacrylamide gels (Planus et al., 1999). Therefore, despite the limitations of transformed cell lines, we considered A549 cells to be a suitable model to study contractile properties of non-migrating alveolar epithelial cells.

4.4.3   Contractile forces exerted by alveolar epithelial cells

Our TM measurements demonstrate that cultured alveolar epithelial cells exhibit contractile tone under basal conditions. Contraction was stronger at the cell periphery, which is consistent with the regional distribution of F-actin cytoskeleton showing a weak rim. The F-actin pattern we found agrees with previous reports of alveolar epithelial cells (Trepat et al., 2005;Kawkitinarong et al., 2004). We quantitatively assessed contraction orientation by computing at each point the direction of the traction vector relative to the centroid of the cell. The histogram of traction angles was very well fitted by a Gaussian function with the addition of a small constant term. The Gaussian distribution was centered around zero with a relatively narrow dispersion, indicating that cell traction forces pull inwards. The constant term accounts for a weak field of forces randomly orientated, which could partially reflect background noise. It should be pointed out that TM measures

the traction forces exerted on the substrate. Therefore, a centripetal force at the cell edge could be generated by radial stress fibers or by a contractile curved rim whose tension results in a net radial component. Alveolar epithelial cells exhibited marked contractile polarity with $M_{xx}/M \sim 3/4$, reflecting a principal traction axis with a contractile moment 3-fold stronger than that of the perpendicular direction. The contractile polarity of alveolar epithelial cells was comparable to that reported on smooth muscle cells (Tolic-Norrelykke et al., 2002). Interestingly, isolated alveolar epithelial cells revealed contractile polarity under symmetrical environmental conditions. Nevertheless, in the alveoli cell contraction polarity might be regulated by cell signaling or structural inhomogeneities. Traction exerted by alveolar epithelial cells was in the range of that reported in endothelial cells (An et al., 2005), suggesting comparable acto-myosin motor activity. On the other hand, forces reported on migrating fibroblasts were ~10-fold higher (Dembo and Wang, 1999). The propulsive forces produced during cell locomotion might explain the stronger tractions exerted on the substrate by migrating cells.

4.4.4 Effect of thrombin on cell contraction and the actin cytoskeleton

Challenge of alveolar epithelial cells with thrombin produced a rapid and marked increase in the cell contractile state, as measured by F, M and maximal local force (Fig. 4.1 and Fig. 4.2). The increase in contraction did not modify the regional distribution of traction forces (Fig. 4.1 and Fig. 4.4) or the contractile polarity. Thrombin exposure resulted in a sharper and narrower distribution of traction angles, indicative of reorientation of traction forces to a more centripetal direction. In agreement with other studies in alveolar epithelial cells (Trepat et al., 2005;Kawkitinarong et al., 2004), thrombin enhanced the peripheral F-actin rim. In addition, we showed that thrombin induces F-actin polymerization (Fig. 4.6). This cytoskeleton remodeling is consistent with the changes in the traction force field exhibited by the cells. Enhancement of traction forces and maintenance of their spatial distribution (Fig. 4.1 and Fig. 4.4) were associated with the formation of peripheral F-actin bundles (Fig. 4.5). This association suggests that cytoskeleton remodeling also contributes to the contractile response induced by thrombin. Disrupting F-actin microfilaments with cytochalasin D resulted in a dramatic fall in traction forces both before and after thrombin addition. Nevertheless, the marked rearrangement

of the actin cytoskeleton with a small reduction in F/G actin ratio indicates that the architecture of the cytoskeleton rather than the amount of polymerized actin plays a pivotal role in contractile force generation.

The enhancement of actomyosin contractile forces induced by thrombin increased prestress as reflected by the rise in M (Wang et al., 2002). The magnitude and time-course of thrombin-induced changes in M parallels the stiffening response recently reported in confluent monolayers of the same cell type (Trepat et al., 2005). Although alveolar epithelial cell stiffening could be a result of actin polymerization and cytoskeleton remodeling (Kole et al., 2004), the comparable increase and temporal correlation between stiffening and contractile responses suggest that the thrombin stiffening effect is dominated by the increase in cell prestress. It has been recently reported that thrombin induces cell stiffening both in confluent and non-confluent monolayers of A549 cells (Trepat et al., 2006). This suggests a thrombin contractile response of A549 cells in confluent monolayers similar to that found in isolated cells.

4.4.5 Activation of pathways signaling MLC phosphorylation by thrombin

Thrombin cleaves protease-activated receptors (PARs) leading to enhanced MLC phosphorylation in alveolar epithelial cells, involving activation of Ca^{2+}/calmodulin-dependent MLCK and inhibition of MLC phosphatase via Rho/Rho kinase pathway (Kawkitinarong et al., 2004). To assess the relative contribution of cytoskeleton rearrangement and MLC phosphorylation to thrombin contractile response of alveolar epithelial cells, we pretreated cells with ML-7 or Y-27623. Inhibition of MLCK with ML-7 dramatically depressed the contractile tone and ablated thrombin-induced contraction (Fig. 7). However, ML-7 caused few changes in actin cytoskeleton (Fig. 4.8) and did not inhibit conversion of G-actin to F-actin produced by thrombin (Fig. 4.6). Therefore, activation of Ca^{2+}/calmodulin-dependent MLCK by thrombin appears to enhance force production in alveolar epithelial cells mostly by acto-myosin interaction with little cytoskeleton remodeling. Inhibition of Rho kinase with Y-27623 also caused contractile tone attenuation and thrombin response ablation. Unlike MLCK, however, inhibition of Rho kinase caused actin remodeling and blocked thrombin-induced F-actin formation, indicating that Rho/Rho kinase pathway mediates actin polymerization and force generation. Taken

together, our findings indicate that activation of PARs by thrombin triggers MLCK and Rho kinase pathways, which remodels the contractile apparatus of alveolar epithelial cells and activates acto-myosin interaction leading to enhanced contraction force.

4.4.6   Force balance in the epithelial monolayer

Cells develop internal tension arising from passive elastic recoil of cytoskeleton filaments and active contraction generated by the acto-myosin molecular motors. Internal tension is partially counterbalanced by microtubules and other intracellular compression-resistive components (Wang et al., 1993). In cell monolayers, the net internal force is counterbalanced by external forces applied at the cell boundary by the adjacent cells and the substrate. Therefore, preservation of the structural integrity of the epithelial cell monolayer lining the alveoli requires cell anchorages to adjacent cells and to the extracellular matrix resist the net traction forces generated by the cell. It should be noted that this is a dynamic force balance since alveolar epithelial cells undergo continuous cyclic stretching caused by breathing. The edemagenic effect of thrombin has been associated with the breakdown of intercellular junctions of the microvascular endothelium caused by the enhancement of active force generation that cell attachments cannot resist (Moy et al., 2002;Dudek and Garcia, 2001). Intercellular gap formation facilitates extravasation of fluid and macromolecules to the interstitial compartment exposing epithelial cells to thrombin. Consistently, elevated levels of thrombin have been found in bronchoalveolar lavage fluid obtained from patients with asthma and acute respiratory distress syndrome (Levi M, 2003;Terada et al., 2004).

In contrast to the fall in TER found in endothelial cells, increased TER has been recently reported in alveolar epithelial cells exposed to thrombin, indicative of improved sealing of the cell monolayer (Kawkitinarong et al., 2004). This suggests that thrombin has two competing effects in the alveolar-capillary barrier function. The thrombin-induced disruption of the endothelial cell barrier has been attributed to a loss of cell-adhesion and to an increase in centripetal contractile forces (Bogatcheva et al., 2002;Dudek and Garcia, 2001;Kawkitinarong et al., 2004;Moy et al., 2002). On the other hand, the barrier protective effect of thrombin observed in epithelial cell monolayers could be a result of a decrease in centripetal forces or an increase in tethering forces (Kawkitinarong et al., 2004). Our study

shows that thrombin increases active centripetal contractile forces generated at the cell periphery in alveolar epithelial cells. In addition, we previously found thrombin-induced stiffening in the same cell type (Trepat et al., 2005). Cell stiffening results in increased passive elastic recoil when the cell is subjected to the breathing stretch which might be locally large in nonhomogenous lung deformation in mechanically ventilated patients with acute lung injury. Thus, thrombin increases both active and passive components of centripetal forces, which favors barrier disruption. Maintenance of the cell monolayer requires cell anchorages to withstand centripetal tension. In our TM experiments, 12% of isolated cells lacking cell-cell attachments exhibited partial detachment from the gel after thrombin challenge. This shows that cell-matrix anchorages alone were not able to resist thrombin-induced contractile forces. In cell monolayers, cell-cell attachments provide additional tethering forces to withstand centripetal tension. Accordingly, the thrombin-induced increase in TER (Kawkitinarong et al., 2004) reported in A459 confluent monolayers indicates that the rise in centripetal tension may be compensated by cell adhesion enhancement, protecting barrier integrity. In this connection, enhanced cortical cytoskeleton and translocation of ZO-1 tight junction protein from the cytosolic compartment to the cell membrane contact sites were also reported in alveolar epithelial cells exposed to thrombin (Kawkitinarong et al., 2004). However, no changes in β-catenin adherens junction protein were found (Kawkitinarong et al., 2004). We have recently reported cell detachment of thrombin treated A549 cells in confluent monolayers when subjected to stretch (Trepat et al., 2006). Cell detachment was substantially impaired in subconfluent monolayers where anchorages to adjacent cells are reduced. Taken together, these findings suggest that cell-cell attachments play a key role in regulating the structural integrity of the alveolar epithelial barrier. Direct measurements of cell-cell and cell-matrix tethering forces are needed to elucidate the effect of thrombin in the mechanical strength of cell attachments. This will require novel methodological approaches to directly probe in intact cell monolayers the adhesion forces imposed by the cells on the matrix and the adjacent cells. It should be noted that reported TER measurements were carried out in confluent cell monolayers under static conditions. However, the rise in elastic recoil caused by cyclic stretch imposes a higher mechanical load onto cell junctions, which might compromise monolayer integrity (Trepat et al., 2006). Importantly, in the damaged alveoli, epithelial cells lose cell-cell contacts, reducing the ability of tethering forces to withstand the increased centripetal tension induced by thrombin. Thus, in the injured lung, thrombin might have an adverse effect on alveolar epithelial monolayer repair.

Chapter 4 Thrombin-induced contraction in alveolar epithelial cells probed by traction microscopy.

In conclusion, we have shown that alveolar epithelial cells exhibit basal contractile tone exerting centripetal traction forces predominantly at the cell periphery. The inflammatory agonist thrombin enhances contraction of alveolar epithelial cells maintaining peripheral and centripetal force distribution. Cell contraction increase is associated with F-actin polymerization and enhancement of the peripheral actin cortex. Contractile response to thrombin is mediated by actin cytoskeleton remodeling and acto-myosin activation through Ca^{2+}/calmodulin-dependent MLCK and Rho/Rho kinase signaling pathways. In the intact alveolar epithelium, the increased contractile centripetal tension may be compensated by cell adhesion tethering forces. However, in the injured lung, thrombin-induced contractile tension might further impair alveolar epithelial barrier integrity.